Journal of Computational Neuroscience manuscript No.
(will be inserted by the editor)

Spatially structured oscillations in a two-dimensional excitatory neuronal network with synaptic depression

Zachary P. Kilpatrick · Paul C. Bressloff

the date of receipt and acceptance should be inserted later

Abstract We study the spatiotemporal dynamics of a two-dimensional excitatory neuronal network with synaptic depression. Coupling between populations of neurons is taken to be nonlocal, while depression is taken to be local and presynaptic. We show that the network supports a wide range of spatially structured oscillations, which are suggestive of phenomena seen in cortical slice experiments and *in vivo*. The particular form of the oscillations depends on initial conditions and the level of background noise. Given an initial, spatially localized stimulus, activity evolves to a spatially localized oscillating core that periodically emits target waves. Low levels of noise can spontaneously generate several pockets of oscillatory activity that interact via their target patterns. Periodic activity in space can also organize into spiral waves, provided that there is some source of rotational symmetry breaking due to external stimuli or noise. In the high gain limit, no oscillatory behavior exists, but a transient stimulus can lead to a single, outward propagating target wave.

Keywords excitatory neuronal network, synaptic depression, oscillations, spiral waves, stationary bumps

Zachary P. Kilpatrick · Paul C. Bressloff
Department of Mathematics, University of Utah, Salt Lake City, UT, 84112-0090

Paul C. Bressloff
Mathematical Institute, University of Oxford, 24-29 St. Giles', Oxford OX1 3LB, UK
E-mail: bressloff@maths.ox.ac.uk

1 Introduction

Spatially localized oscillations arise both *in vivo* and *in vitro* and may be observed experimentally using multi–electrode arrays or voltage–sensitive dye imaging [62]. Such organizing activity in the brain has been purported to play a role in sensory perception [13, 31], memory – both working and long term [27], and pathological events like epilepsy [38]. Whether or not large-scale brain oscillations are epiphenomena or have functional significance remains an open question in many cases. However, both experiment and modeling continue to devote efforts to understanding the mechanisms that generate and sustain oscillations [7].

When neocortical or hippocampal *in vitro* slices are treated with an inhibitory neurotransmitter antagonist such as bicuculline, effectively eliminating inhibition, a localized current stimulus evokes population activity. Such activity may take the form of a spatially localized group of neurons whose population activity oscillates around 1–10Hz [60, 38, 50]; during each oscillation cycle the population may emit elevated activity that propagates as a traveling pulse [60, 9, 62] or a spiral wave [23, 48]. Spiral waves provide a mechanism for spatially organizing extensive episodes of periodic activity, effectively reducing the dimensionality of the dynamics [48]. Since inhibitory connectivity is pharmacologically blocked, any negative feedback in the network is likely to arise at the single cell level due to mechanisms such as synaptic depression [1, 4, 35, 53, 57] and spike frequency adaptation [5].

A variety of sensory stimuli have been linked to oscillations *in vivo*. For example, a number of stud-

ies of vertebrate and invertebrate olfactory bulbs have found that odor stimuli can elicit oscillations [32, 10]. Stimuli can also evoke oscillations and waves in visual cortex [51, 45, 63, 6, 20], rat barrel cortex [41], and auditory cortex [31]. Spatiotemporal activity is not only a neural correlate of sensory stimuli, but is also associated with various forms of memory. For example, the encoding of new information as well as the retrieval of long-term memory is reflected by the period of oscillations [27], and the recall of a previous memory is often accompanied by an increase in oscillatory power [49]. On the other hand, stationary bumps of persistent spatial activity that neither propagate nor oscillate have been seen during working memory tasks [59].

Oscillations can also be the signature of certain brain pathologies such as epilepsy [38]. Electrophysiology has been used to study epilepsy in humans as well as animal models, and seizures are usually accompanied by measurable stuctured population activity. Trauma or developmental malfunction can lead to reduced regions of inhibition, axonal sprouting, or synaptic reorganization of excitatory circuitry [11]. Such regions are prime candidates for epileptic seizure foci. Any incurring excitatory input may be sufficient to create high frequency oscillations in the population activity of these patches of cortex [36]. The nature of such structured population activity as recorded by electroencephalagram can indicate the nature of the seizure mechanism [33]. As in cortical slice studies, some seizures have hallmark electrical activity traces consisting of focused localized synchronous oscillations that emit traveling pulses [47].

In light of the above examples, it is important to understand the mechanisms behind spatially structured oscillations in large scale neuronal networks due to their functional and pathological implications. A number of organizing mechanisms for such spatiotemporal activity have been suggested, including a single pacemaker oscillator exciting successive neighbors in an excitable network, or coupled oscillators propagating gradual phase delays in space [13, 62]. Therefore, activity that propagates away from a focused region of high frequency oscillations may either travel faster than the characteristic time-scale set by the oscillating region, according to dynamics of an excitable medium, or at a speed set by the period of the oscillating core if the rest of the medium is oscillatory as well. Conceivably, this may establish a dynamical systems explanation for the wide range in speed at which seizures spread across the cortex, which can be anywhere from 0.05mm/s to 10cm/s [38].

Recently Troy and Shusterman [54] have shown how a pulse emitting oscillating core can occur in an excitatory neuronal network based on a neural field model with linear negative feedback [42]. They first considered a two–dimensional network operating in an excitable regime with a homogeneous low activity (Down) state that corresponded to a stable fixed point of the space–clamped dynamics. Linearization about the fixed point yielded a Jacobian with complex eigenvalues so that the fixed point was a stable focus. In this regime, Troy and Shusterman showed that after breaking the rotational invariance of an initally generated target wave, reentry of the free ends of the resulting rotor into the center of the domain generated subsequent waves. In the same system, spiral waves were generated by periodically breaking rotational invariance with an inhibitory stimulus. In a subsequent study they showed that the same system, with large enough negative feedback, supports spatially localized oscillations that periodically emit traveling pulses [50]. In this regime the space–clamped model exhibits bistability, in which a stable Down state coexists with a stable limit cycle. However, since the linear form of adaptation used in these studies is not directly related to physiological models of adaptation, it is difficult to ascertain whether or not the levels of feedback required are reasonable.

In this paper, we show how various forms of spatially structured oscillations, including spiral waves and pulse emitters, can occur in a two dimensional excitatory neuronal network with a physiologically based form of nonlinear negative feedback, namely, synaptic depression. Previously, we considered the combined effects of synaptic depression and spike frequency adaptation on the spatiotemporal dynamics of a one–dimensional excitatory network [26]. We showed that synaptic depression tends to dominate the dynamics, providing a mechanism for generating spatially localized oscillations. Here we extend our analysis to two dimensions and to the case of noisy networks. For simplicity, we ignore the effects of spike frequency adaptation since they tend to be relatively weak. The basic two–dimensional model is introduced in section 2. We then analyze the space–clamped version of the model, and show that it supports a stable limit cycle in the absence of noise (section 3). However, in the presence of additive white noise,

the parameter regime over which oscillations can occur can be significantly widened. In section 4 we present a number of numerical simulations illustrating various two–dimensional spatiotemporal activity patterns supported by the full network model. Depending on the initial conditions, we show that in the absence of noise, network activity can evolve as a pulse-emitting oscillating core or as a spiral wave. Furthermore, addition of a small amount of spatially uncorrelated noise to a quiescent network can drive pockets of the system superthreshold and lead to discrete locations of pulse-emitting cores. On the other hand, large amounts of noise lead to bulk oscillations which can disrupt any spatially structured activity. We also show that when a radially symmetric stimulus is applied to the network in the presence of noise, spiral waves can be generated due to symmetry breaking, similar to the organized activity found in mammalian cortical slice [23, 48]. Finally, we study the system in the high–gain limit (section 5). In this case, oscillations do not exist in the deterministic system, but depression is a sufficient mechanism for generating outward propagating target waves following a brief stimulus.

2 Neural network model with synaptic depression

We consider a neuronal network model which includes synaptic depression [1, 4, 35, 53, 57, 64]. As opposed to the usual Pinto-Ermentrout formulation of negative feedback [42, 14, 54, 55] in spatially extended neural fields, here we take negative feedback to depend on output firing rate

$$\frac{\partial u(\mathbf{r},t)}{\partial t} = -u(\mathbf{r},t) + w * (qf(u))\,(\mathbf{r},t) \tag{2.1a}$$

$$\frac{\partial q(\mathbf{r},t)}{\partial t} = \frac{1-q(\mathbf{r},t)}{\alpha} - \beta q(\mathbf{r},t) f(u(\mathbf{r},t)), \tag{2.1b}$$

where

$$w * (qf(u))\,(\mathbf{r},t) = \int_{\mathbb{R}^2} w(|\mathbf{r}-\mathbf{r}'|) q(\mathbf{r}',t) f(u(\mathbf{r}',t)) \mathrm{d}\mathbf{r}'$$

where $\mathbf{r}$ and $\mathbf{r}'$ are spatial positions in the two-dimensional plane $\mathbb{R}^2$. Equation (2.1a) describes the evolution of the synaptic current or drive $u(\mathbf{r},t)$ in the presence of synaptic depression, which takes the form of a synaptic scaling factor $q(\mathbf{r},t)$ evolving according to equation (2.1b). The factor $q(\mathbf{r},t)$ can be interpreted as a measure of available presynaptic resources, which are depleted at a rate βf [57, 4, 53], and are recovered on a timescale specified by the constant α (experimentally shown to be 200-1500ms [1, 56, 57, 52]). In a previous study, we considered a one-dimensional model with synaptic depression and adaptation and showed that adaptation has a relatively small effect on the dynamics [26]. Therefore, we focus on synaptic depression here. It will be convenient in the following to fix parameters so that f is interpreted as the fraction of the maximum firing rate, that is $0 \leq f \leq 1$.

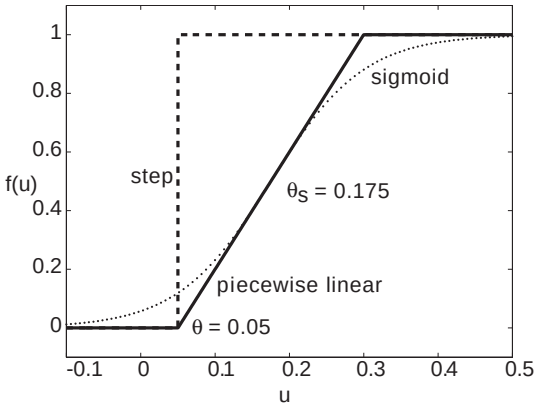

Fig. 1 Comparison of the step, piecewise linear, and sigmoid firing rate functions. Parameter values are $\theta = 0.05$ and $\sigma = 4$. The sigmoid function has the same slope and value as the piecewise linear function at their mean values. When compared to the sigmoid function, it is apparent that the piecewise linear function's true threshold is more accurately given by $\theta_s = 0.175$, rather than θ, the point at which nonzero firing occurs.

Most of our analysis and numerics are carried out for a general piecewise linear firing rate function that attains saturation as pictured in Fig. 1:

$$f(u) = \begin{cases} 0, & u \in (-\infty, \theta), \\ \sigma(u-\theta), & u \in (\theta, \theta+\sigma^{-1}), \\ 1, & u \in [\theta+\sigma^{-1}, \infty). \end{cases} \tag{2.2}$$

Here σ specifies the slope of the linear regime. (One could also consider a firing rate function with a step followed by linear increase [18, 19]). Note that taking the firing rate to be a linear function close to threshold is consistent with the observation that spike frequency adaptation tends to linearize the firing frequency-input current curve [12, 58]. In the limit that $\sigma \to \infty$, we recover the Heaviside step function used in Amari's original work on scalar networks [2] and most analytical studies of the Pinto-Ermentrout model [42, 43, 50, 14, 16, 15, 54, 55]:

$$f(u) = H(u-\theta) = \begin{cases} 0, & u \in (-\infty, \theta), \\ 1, & u \in [\theta, \infty). \end{cases} \tag{2.3}$$

We will use such a function in order to study target waves and stationary bumps (see section 5). One

important point, as illustrated in Fig. 1, is that the threshold θ in equation (2.2) is not necessarily analogous to the threshold θ in equation (2.3). A region above threshold in the piecewise linear case might still be considered "off" if it only sustains a low level of activity. This is further reinforced by comparison with a sigmoid function in which threshold is taken to be the point at which the firing rate is half its maximum value:

$$f(u) = 1/(1 + \exp(-\sigma(u - \theta_s))). \tag{2.4}$$

The homogeneous weight distribution $w(|\mathbf{r} - \mathbf{r}'|)$ defines the strength of the synaptic connections between neurons at $\mathbf{r}$ and $\mathbf{r}'$, depending only on the distance between two cells. Typical excitatory weight functions are monotone decreasing functions such as the exponential and the Gaussian. We will take w to be given by a difference of modified Bessel functions of the second kind: [14, 29, 40]

$$w(r) = \frac{2w_0}{3\pi d}\left(K_0(r/d) - K_0(2r/d)\right), \tag{2.5}$$

where w_0 determines the strength of the synaptic connections. The factor $2/3\pi$ ensures that equation (2.5) is a very good fit to the exponential weight function

$$w(r) = \frac{w_0}{2\pi d}\mathrm{e}^{-r/d}$$

The expansion in terms of Bessel functions is particularly convenient because it allows us to transform the system (2.1) into a fourth order PDE, which is computationally less expensive to simulate [28, 29, 54, 40] (see section 4). Finally, we fix the temporal and spatial scales of the network by setting $\tau = 1$ and $d = 1$. The membrane time constant is typically around 10 ms, whereas the range of synaptic connections within cortex is of the order 1 mm. We also fix synaptic strength by setting $w_0 = 1$. The effects of varying w_0 are briefly discussed at the end of section 3.

3 Oscillations in the space-clamped system

Previous modeling studies of space-clamped neuronal networks with synaptic depression showed the existence of oscillations in the case of excitatory/inhibitory networks [57] or for a purely excitatory network with noise [4]. Tabak *et. al.* showed that an excitatory network with depression could support regular oscillations and bursting, using an alternative form for the neural field equation as well as different gains and thresholds for each variable's activation function [53]. In our study, we find that saturation of the activation function is sufficient to stabilize limit cycles using the same activation function for both the activity and depression variables.

3.1 Phase plane for piecewise linear firing rate

As a means of determining the oscillatory behavior of the system, we examine the equilibria of the space-clamped system [4, 53, 57]

$$\begin{aligned} \dot{u}(t) &= -u(t) + q(t)f(u(t)), \\ \alpha\dot{q}(t) &= 1 - q(t) - \alpha\beta q(t)f(u(t)), \end{aligned} \tag{3.1}$$

where f is the piecewise linear activation function (2.2) shown in Fig. 1. We carry out the stability analysis of phase space using the piecewise linear function because explicit analytical expressions can be derived for the fixed points. However, these results extend to the case where there is a smooth transition from the linear to the saturated portion of the firing rate.

To calculate equilibria of (3.1), we consider the possible solutions on the three domains of the piecewise function $f(u)$. We find that there is a low activity or Down state on the lower domain ($u < \theta$) for $\theta > 0$ such that $(u, q) = (0, 1)$. The stability of this Down state is determined by the eigenvalues of the Jacobian

$$\mathcal{J}(0,1) = \begin{pmatrix} -1 & 0 \\ 0 & -1/\alpha \end{pmatrix} \tag{3.2}$$

and is therefore stable for all realistic parameters. A stable Down state exists in the network for any f with a hard threshold, that is $f(u) = 0$ for $u < \theta$. Without this condition, it is possible that the Down state may destabilize or vanish due to a nonzero firing rate existing for zero synaptic drive.

We find additional equilibria by solving (3.1) on the middle and upper domains of f. On the middle domain ($\theta \le u \le \theta + \sigma^{-1}$), where $f(u) = \sigma(u - \theta)$, we have

$$u = \sigma(u - \theta)q, \tag{3.3}$$

$$q = 1/(1 + \sigma\alpha\beta(u - \theta)), \tag{3.4}$$

$$\theta \le u \ \le \ \theta + \sigma^{-1}, \tag{3.5}$$

which has solutions

$$u = \frac{\sigma + \sigma\alpha\beta\theta - 1 \pm \sqrt{\mathcal{D}}}{2\sigma\alpha\beta} \tag{3.6}$$

$$q = \frac{2}{1 + \sigma - \sigma\alpha\beta\theta \pm \sqrt{\mathcal{D}}} \tag{3.7}$$

$$\mathcal{D} = (\sigma + \sigma\alpha\beta\theta - 1)^2 - 4\sigma^2\alpha\beta\theta$$

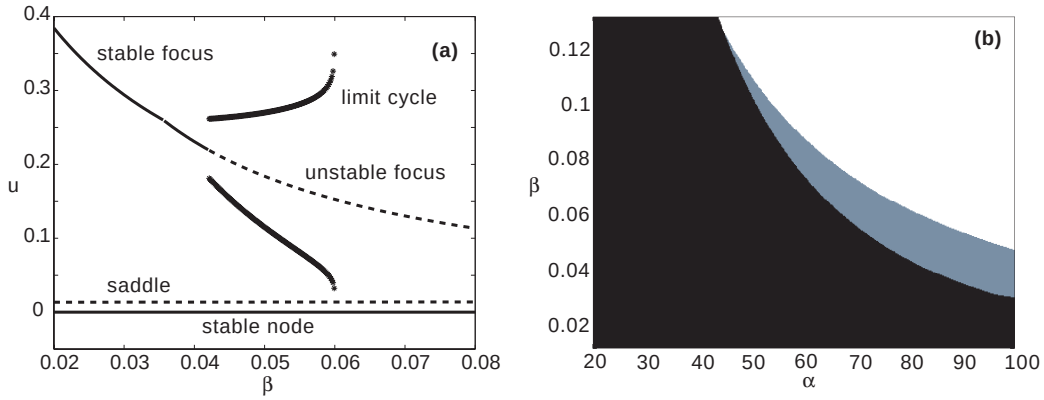

Fig. 2 (a) Bifurcation diagram showing fixed points u of the system (3.1) as a function of β for $\alpha = 80$. (b) Stability diagram for the space–clamped system (3.1) showing regions in parameter space where the Up state is a stable focus (black), an unstable focus surrounded by a stable limit cycle (grey), or an unstable focus without a limit cycle (white) . Other parameters are $\theta = 0.01$, and $\sigma = 4$.

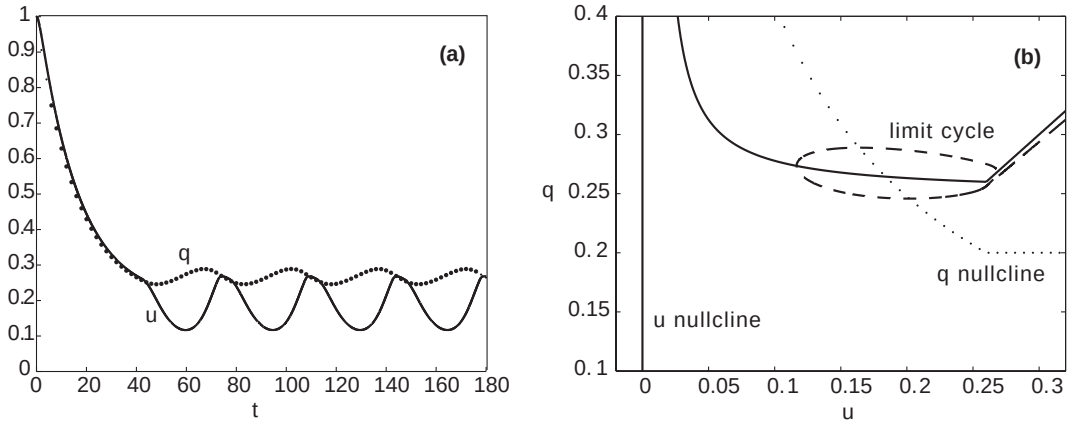

Fig. 3 (a) Numerical simulation of (3.1) using the parameters $\theta = 0.01$, $\sigma = 4$, $\alpha = 80$, and $\beta = 0.05$ given the initial condition $(u,q) = (1,1)$. The synaptic input u and fraction of available resources q are plotted as a function of time t. Oscillations lock to a period roughly determined by the time constant α. (b) Corresponding phase–plane plot of q versus u (dashed line) showing that the system supports a stable limit cycle.

provided $\mathcal{D} \geq 0$ and condition (3.5) is satisfied. Stability is determined by the eigenvalues of the Jacobian

$$\mathcal{J}(u,q) = \begin{pmatrix} -1+\sigma q & \sigma(u-\theta) \\ -\beta\sigma q & -(1/\alpha + \beta\sigma(u-\theta)) \end{pmatrix}. \quad (3.8)$$

We find that for a wide range of parameters, the middle domain contains two equilibria, one of which is a saddle and the other is a stable or unstable focus. The latter corresponds to a high activity or Up state. For sufficiently fast depression, destabilization of the Up state can lead to the formation of a stable limit cycle via a subcritical Hopf bifurcation as pictured in Fig. 2. In parameter regimes where the focus equilibrium does not exist, the Up state occurs on the upper domain ($u > \theta + \sigma^{-1}$), where $f(u) = 1$, and is given by

$$u = 1/(1+\alpha\beta), \quad (3.9)$$

$$q = 1/(1+\alpha\beta), \quad (3.10)$$

Its stability is determined by the eigenvalues of the Jacobian

$$\mathcal{J}(u,q,a) = \begin{pmatrix} -1 & 1 \\ 0 & -(1/\alpha+\beta) \end{pmatrix}, \quad (3.11)$$

which guarantees that such an Up state is always stable.

In Fig. 3 we show a simulation of the space-clamped network for a choice of parameters that supports a limit cycle. The parameter value for synaptic depression time constant α is taken to be within the physiological range 200-1500ms [1, 57]. Notice that both variables oscillate at a period of roughly 40 time units or 400ms, which cor-

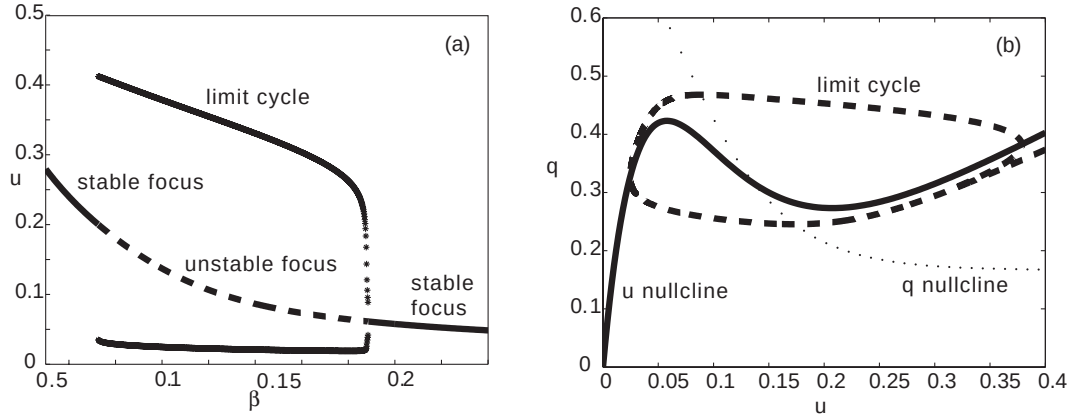

Fig. 4 (a) Bifurcation diagram showing fixed points u of the system (3.1) as a function of β for $\alpha = 50$. (b) Phase–plane plot of q versus u (dashed line) showing the system supports a limit cycle. Other parameters are $\theta_s = 0.15$, and $\sigma = 20$.

relates well with the scale of epileptiform events [8, 36, 38, 50]. This also implies that the timescale of oscillations is roughly set by the time constant of synaptic depression. Notice that as opposed to self sustained oscillations in the Pinto-Ermentrout model [50], the equilibrium focus in our model is associated with the Up rather than the Down or rest state. As stated, these results easily extend to the case where f is a smooth, saturating function above the threshold value $u = \theta$. In particular, since limit cycles are structurally stable solutions in continuous systems, oscillations persist when $f(u)$ is modified by smoothing out the corner at $u = \theta + 1/\sigma$. However, without a hard threshold at $u = \theta$, we have not witnessed the same types of dynamics as presented here for the piecewise linear f. If oscillations exist, a stable Down state does not, which we show in an analysis of the system with a sigmoidal firing rate function (2.4).

3.2 Phase plane for sigmoidal firing rate

We use a numerical root finding algorithm to identify the equilibria of the system (3.1) in the case where f is the sigmoidal function (2.4). It is possible to find physiologically reasonable parameter regimes where limit cycles exist, but they do not appear to coincide with a stable Down state, as in the piecewise linear f case. We show an example of one such limit cycle in Fig. 4, where transitions between low and high activity states occur at the knees of the u-nullcline . There is no such mechanism in the limit cycle present in the piecewise linear system. This distinction suggests that the loss of a hard threshold may change the overall topology of dynamics within the network. Rather than finding an excitable regime with limit cycles about the Up state, we find either a purely oscillatory regime, or an excitable regime with no limit cycles.

3.3 Space–clamped system with noise

A previous study of the space–clamped system (3.1) with f given by (2.2) considered parameter regimes in which the subcritical Hopf bifurcation of the Up state only produced an unstable limit cycle [4]. In this case the authors showed that oscillations could be generated in the presence of additive noise, which switched the system between the Up and Down states (see also [22]). It follows that noise enlarges the parameter regime over which self-sustained oscillations can occur. We illustrate the effects of additive noise by simulating the system

$$\begin{aligned} \dot{u}(t) &= -u(t) + q(t)f(u(t)) + \gamma\nu(t), \\ \alpha\dot{q}(t) &= 1 - q(t) - \alpha\beta q(t)f(u(t)), \end{aligned} \tag{3.12}$$

where f is the piecewise linear function (2.2), $\nu(t)$ is a Gaussian white noise process such that $\langle\nu(t)\rangle = 0$, and $\langle\nu(s)\nu(t)\rangle = 2\delta(t-s)$; γ is the noise strength. We simulated the system (3.12) using an Euler-Maruyama scheme for stochastic differentiation with a timestep $\Delta t = 10^{-6}$. The nature of the noise–induced oscillations depends upon whether the Up state is a stable or unstable focus. In the case of a stable focus, even though oscillations are damped out eventually in the deterministic system, noise is sufficient to repeatedly drive the system between the Up and Down states, along analogous lines to [4]. However, the oscillations tend to be rather irregular as illustrated in Fig. 5.

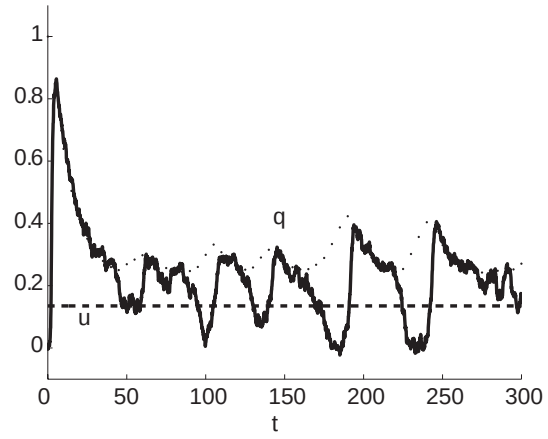

Fig. 5 Numerical simulation of the space–clamped system (3.12) in which background noise drives the system between Up and Down states. The horizontal dashed line denotes the input current value at which activity is half of its maximal value ($\theta_s = 0.135$). Firing rate is taken to be piecewise linear function (2.2). Parameters are $\alpha = 60$, $\beta = 0.06$, $\gamma = 0.02$, $\theta = 0.01$, and $\sigma = 4$. In the absence of noise, the Up state is a stable focus.

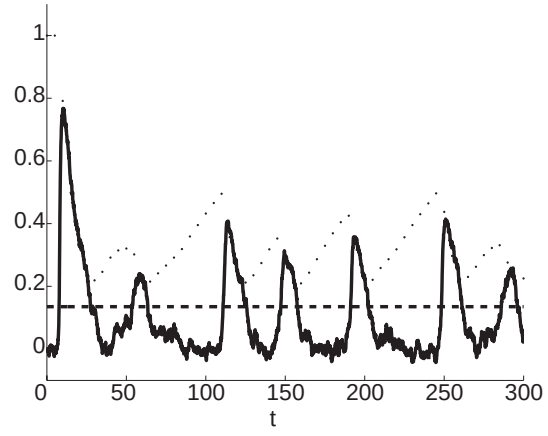

Fig. 6 Same as Fig. 5 except $\alpha = 80$ so that now the Up state is an unstable focus in the absence of noise.

More regular noise–induced oscillations occur in the case of an unstable focus. Equations (3.12) now represent an excitable system with only a stable Down state, in which noise periodically drives the system above threshold, leading to an elevated firing rate that then relaxes back down as synaptic depression is activated. An example simulation is shown in Fig. 6, which neatly illustrates the regularity of the noise–induced oscillations. This is an example of a well known stochastic property of excitable systems, namely, coherence resonance [34]. That is, there exists an optimal level of noise with respect to the degree of regularity of the induced oscillations; if the level of noise is too high then this completely washes out any oscillations. We conclude that noise extends the parameter range over which the space–clamped system supports oscillations to include regions where the underlying deterministic system supports a stable or unstable focus without a stable limit cycle. This also has important implications for the effects of noise in the spatially extended system (see section 4).

Bart *et. al.* [4] showed that changing the synaptic strength w_0 can also alter the stability of the Up state of the system (3.1), whilst keeping all other parameters fixed. Stronger synapses (higher w_0) stabilize the Up state, while weaker synapses (lower w_0) destabilize it. Consistent with these observations, we found that changing w_0 alters the parameter ranges of α and β over which a stable limit cycle exists. That is, increasing w_0 shifts the region in which limit cycles exist to higher values of α. On the other hand, decreasing w_0 allows for limit cycles to exist for lower values of α, but the range of β values over which they exist is much narrower. Thus, superthreshold activity in a network with weak synapses is much more easily overridden by synaptic depression. In our simulations we take $w_0 = 1$.

4 Oscillations in the spatially extended model

We now consider the implications of the existence of deterministic and noise-induced oscillations in the splace–clamped model for spatially structured oscillations in the full model (2.1). Using numerical simulations, we demonstrate that the two dimensional network supports a spatially localized oscillating core that emits target waves each cycle, as well as spiral waves. The results presented here can also be generated for a system with smoother forms of f. However, as the simulations are qualitatively similar, we only show results for the piecewise linear case. As in previous studies of two-dimensional neural field models, we carry out a transformation of our system for more efficient computation [28, 29, 54, 40]. That is, we convert the integro-differential equation system (2.1) to a fourth order PDE using two-dimensional Fourier transforms. This is possible due to the fact that the Fourier transform of the weight distribution $w(\mathbf{r}, \mathbf{r}')$ given by equation (2.5) is a rational function. Discretizing the resulting differential operators leads to sparse matrices, as opposed to full matrices arising from an integral operator.

Numerical simulations are thus performed on the following system, which is equivalent to equa-

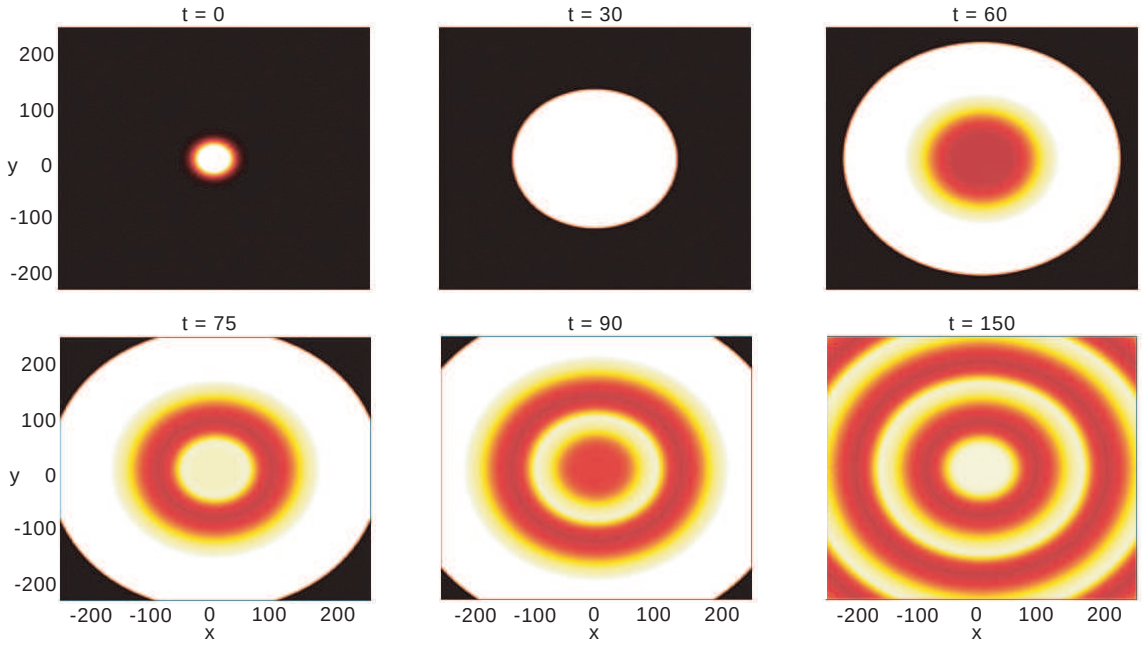

Fig. 7 Snapshots of the solution $u(x, y, t)$ to the fourth order PDE (4.1), following a stimulus specified by equation (4.3) at $t = 0$, where $\chi = 1$ and $\zeta = 25$. Initially, an activated state spreads radially outward, across the entire medium as a traveling front. Then, the localized oscillating core of activity emits a target wave with each oscillation cycle. Eventually, these target waves fill the domain. Each target wave can be considered as a phase shift in space of the oscillation throughout the medium; they travel with the same speed as the initial front. Parameters are $\alpha = 80$, $\beta = 0.05$, $\sigma = 4$.

tions (2.1) and (2.5):

$$\left[\nabla^4 - A\nabla^2 + B\right](u_t + u) = Mqf(u),$$
$$q_t = \frac{1-q}{\alpha} - \beta q f(u) \quad (4.1)$$

over the domain $\Omega \subset \mathbb{R}^2$. Here, the fourth order operator, $\mathcal{L} = \nabla^4 - A\nabla^2 + B$, arises as the denominator of the two–dimensional Fourier transform of our modified Bessel weight function (2.5), which is given by

$$\hat{w}(\rho) = \frac{2}{3\pi}\left(\frac{1}{\rho^2+1} - \frac{1}{\rho^2+2^2}\right) = \frac{2/\pi}{\rho^4 + 5\rho^2 + 4}, \quad (4.2)$$

where $\hat{\cdot}$ denotes the two-dimensional Fourier transform. In this case, $A = 5$, $B = 4$, and $M = 2/\pi$, but we may adjust these parameters by considering a rescaling of w. We solve the system (4.1) numerically on a Cartesian grid of 1000×1000, applying homogeneous Dirichlet and Neumann boundary conditions. For the fourth order operator, we employed a second order finite difference method to construct a matrix version of $\mathcal{L}$. The time derivative was approximated using forward Euler with a timestep of $\Delta t = 0.01$, which was small enough so that shrinking it further did not change results.

4.1 Pulse emitter

Similar to our previous study of a one-dimensional network [26], we find that in parameter regimes where a stable limit cycle exists in the space-clamped system, the corresponding two–dimensional network supports a spatially localized oscillating core that periodically emits traveling pulses. All that is necessary to induce such behavior is an initial condition of the form

$$(u(\mathbf{r}, 0), q(\mathbf{r}, 0)) = (\chi e^{-(x^2+y^2)/\zeta^2}, 1), \quad (4.3)$$

where χ and ζ parameterize the amplitude and spatial constant of the initial state. We seek to characterize the evolving activity in the limit cycle regime, especially the period of oscillation and the speed of emitted pulses. In Fig. 7, we show an example of a pulse-emitting core, which oscillates at a frequency of roughly 3Hz. Pulses are emitted each cycle, and travel at a speed of roughly 30cm/s, which is determined by the period of the oscillations; the latter is set by the time constant of synaptic depression. The initial emission of spreading activity appears as a traveling front which propagates from the region activated by the input current into the surrounding region of zero activity; it travels at the same speed as the subsequent target waves. The front converts each region of the net-

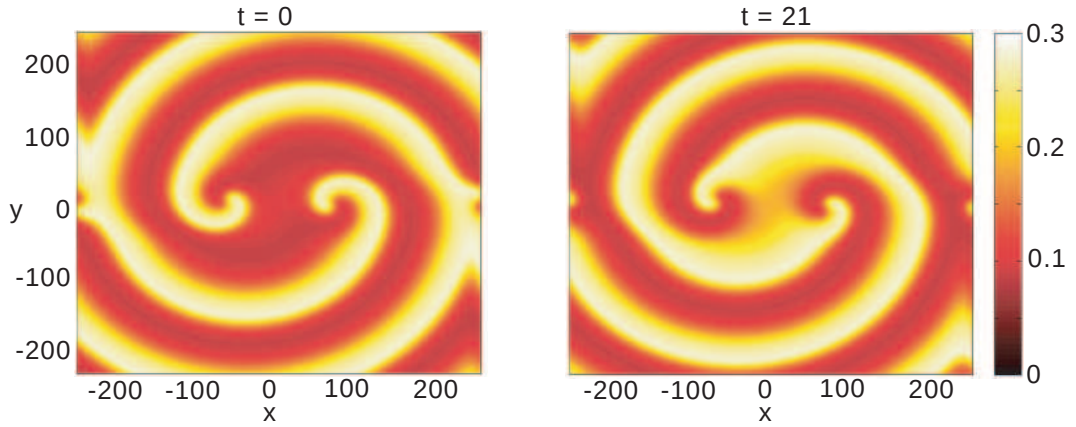

Fig. 8 Snapshots of a solution $u(x, y, t)$ to the fourth order PDE (4.1) revealing the counter-rotation of two spiral waves on either side of the domain. These were generated with an initial condition where the target pattern of Fig. 7 had the top and bottom halves of the domain phase shifted. Parameters are $\alpha = 80$, $\beta = 0.05$, $\sigma = 4$, and $\theta = 0.01$.

work into an oscillatory state that is phase–shifted relative to the core, resulting in the appearance of a radially symmetric target pattern. Since our network has solely excitatory connections, we can consider it to be akin to disinhibited neocortical or hippocampal slices [9, 60, 62] or regions of cortex or hippocampus where excitatory circuitry dominates due to some pathology [8, 11]. Interestingly, the speed of the simulated waves matches the timescale of fast seizure spread in cortex [38].

4.2 Spiral waves

Several experimental and modeling studies of two-dimensional cortex reveal the existence of spiral waves [23, 29, 38, 47, 48]. Such self-sustained activity can often be classified by a constant angular velocity [23, 47]. When identified using voltage sensitive dye, one finds such activity patterns have true phase singularities about which the spiral organizes. One may think of such spatially structured activity as a network property manifesting the recovery period necessary for groups of neurons. Therefore, sections of cortex about the phase singularity alternate between Down and Up states, giving ample time for sections to recover during the Down state.

Spiral waves have been generated in previous studies of neural field models with linear adaptation, in which the neuronal network acts like an excitable medium [29, 54]. The oscillations necessary for the generation of spiral waves arise from the Down state of the network being a stable focus. Laing used the rotational symmetry of the spiral waves to generate equations for the activity profile and angular velocity of a spiral on a disc domain [29]. Troy and Shusterman generated spiral waves by continually breaking the symmetry of target waves in the network [54]. In our model, we find that spiral wave patterns can be induced by breaking the rotational symmetry of pulse emitter solutions. More specifically, we chose an initial condition where the target pattern produced by the emitter has the top and bottom halves of its domain phase shifted. The network then evolves into two counter-rotating spirals on the left and right halves of the domain as shown in Fig. 8. Closer inspection of one of these spirals reveals that it has a fixed center about which activity rotates indefinitely as shown in Fig. 9.

Huang and others showed that spiral waves generated in cortical slices are a way for oscillating activity to organize spatially in a smooth and isotropic medium [23]. They found the waves persisted for up to 30 cycles and rotated at a rate of roughly 10 cycles per second. Also, the phase singularity at the center of a spiral wave experiences a reduction in oscillation amplitude due to the mixing of all phases in a small region. Certainly, the spiral waves we have found in our system persist for a long time, but it seems that the rotation rate is slightly slower at roughly 2Hz. Of course this is due in part to the time constant of synaptic depression. As we have shown in our previous work, including spike frequency adaptation can increase the frequency of oscillations [26].

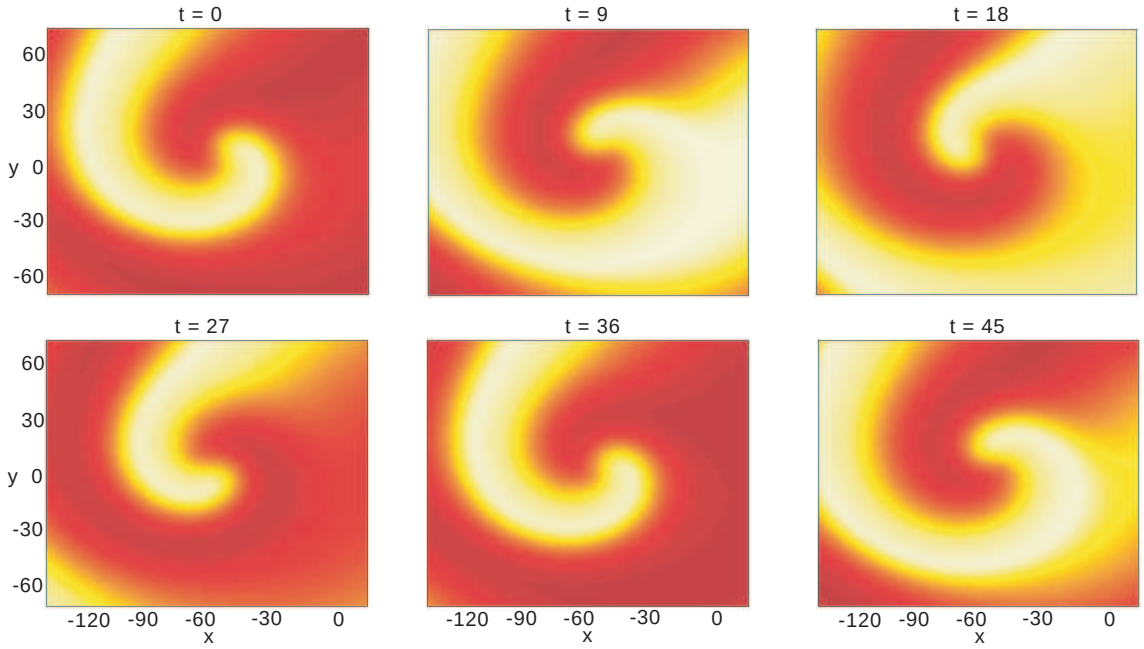

Fig. 9 A zoomed in version of the rotating left spiral wave pictured in Fig. 8. The period of the spiral wave oscillation is roughly the same as the period of the oscillation in the space-clamped system. All patches of neurons are oscillating at the same frequency, but phase-shifted as coordinates are rotated about the central phase singularity. Parameters are $\alpha = 80$, $\beta = 0.05$, $\sigma = 4$, and $\theta = 0.01$.

4.3 Noise–induced oscillations

As in the space-clamped system, it is interesting to consider the effects of noise on the two–dimensional spatially extended network. In a recent study of the role of additive Gaussian noise on Turing instabilities in neural field equations, Hutt *et. al.* found that noise delays the onset of pattern formation [24]. Also, Laing *et. al.* have shown that in a neural field model with linear adaptation, moving bumps are slowed by the introduction of an additive noise term [30]. Here we show that in addition to modulating spatiotemporal activity patterns that exist in the deterministic system, noise also gives rise to new dynamics.

Following a previous study of neural field models with additive noise [30], we introduce a Gaussian white noise term to each equation of a discretized version of the fourth order PDE (4.1):

$$\mathcal{L}_h\left(\frac{u_{ij}^{k+1}-u_{ij}^{k}}{\Delta t}+u_{ij}+\eta\mu_{ij}(t)\right)=Mq_{ij}f(u_{ij}),$$

$$\frac{q_{ij}^{k+1}-q_{ij}^{k}}{\Delta t}=\frac{1-q_{ij}}{\alpha}-\beta q_{ij}f(u_{ij}), \qquad (4.4)$$

where $i = 1, ..., N_x$ and $j = 1, ..., N_y$, $\mathcal{L}_h$ is the finite difference version of the linear operator given in equation (4.1) , u_{ij} and q_{ij} are discrete values of u and q at $(x, y) = (x_i, y_j)$, each μ_{ij} evolves independently as $\langle\mu_{ij}(t)\rangle = 0$ and $\langle\mu_{ij}(t)\mu_{ij}(s)\rangle = \delta(t-s)$, and η is the variance of our white noise term.

In the case of low levels of spatially incoherent Gaussian noise, we find that small pockets of the network spontaneously form spatially localized oscillators which then interact with one another via the target waves that propagate from their cores. We picture this in Fig. 10 for $\eta = 0.005$. Therefore, as in the space-clamped case, noise provides a mechanism for generating oscillations in a situation where the deterministic system would remain quiescent. If the noise level is increased then it tends to disrupt these oscillating cores, which provides a symmetry breaking mechanism for the generation of spiral waves as illustrated in Fig. 11. Following induction of a spatially localized oscillation using a Gaussian stimulus of the form (4.3), we find that the oscillating core begins to be broken up by the noise such that the two halves of the core oscillate antisynchronously. A semi-ring wave then propagates from the bottom to the top of the domain (first three snapshots in Fig. 11), and breaks up into two spiral waves as it reaches the boundary of the core (fourth snapshot). Background oscillations absorb the two spiral waves and the ring-wave is reinitiated (final two snapshots). At even higher levels of noise any spatially struc-

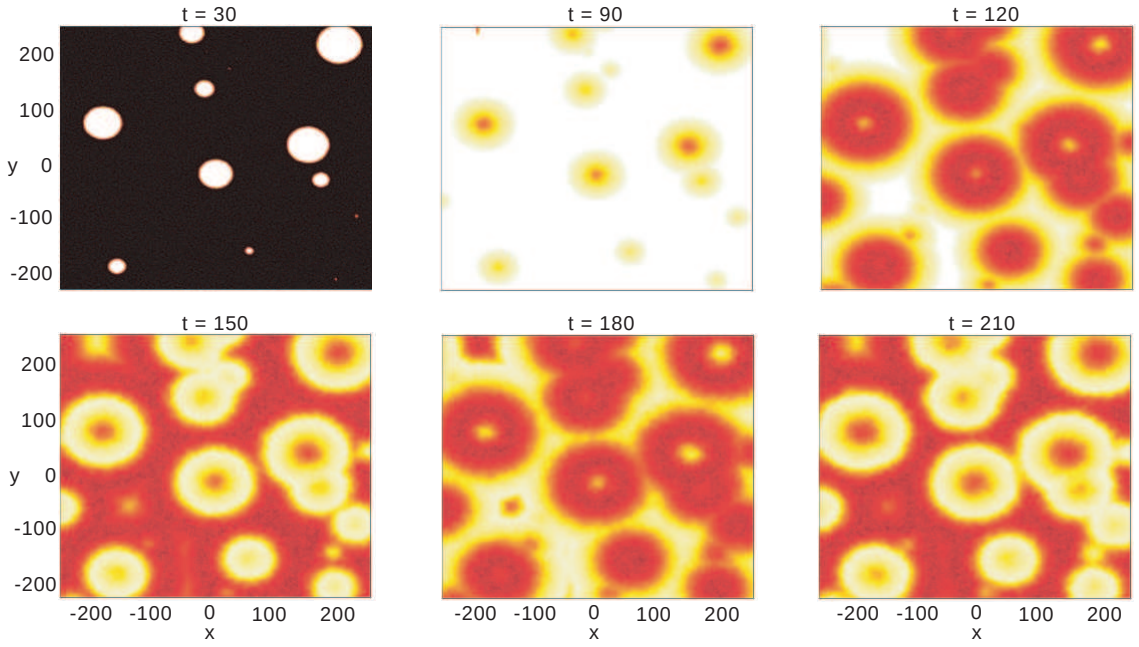

Fig. 10 Snapshots of a solution $u(x, y, t)$ to the noisy system (4.4) in the absence of stimulation. Background noise initiates spatially localized oscillating cores at discrete sites in the medium. Target waves emitted by the various oscillating regions collide, disrupting the spatial structure of the oscillations. Parameters are $\alpha = 80$, $\beta = 0.05$, $\eta = 0.005$, $\sigma = 4$, and $\theta = 0.01$.

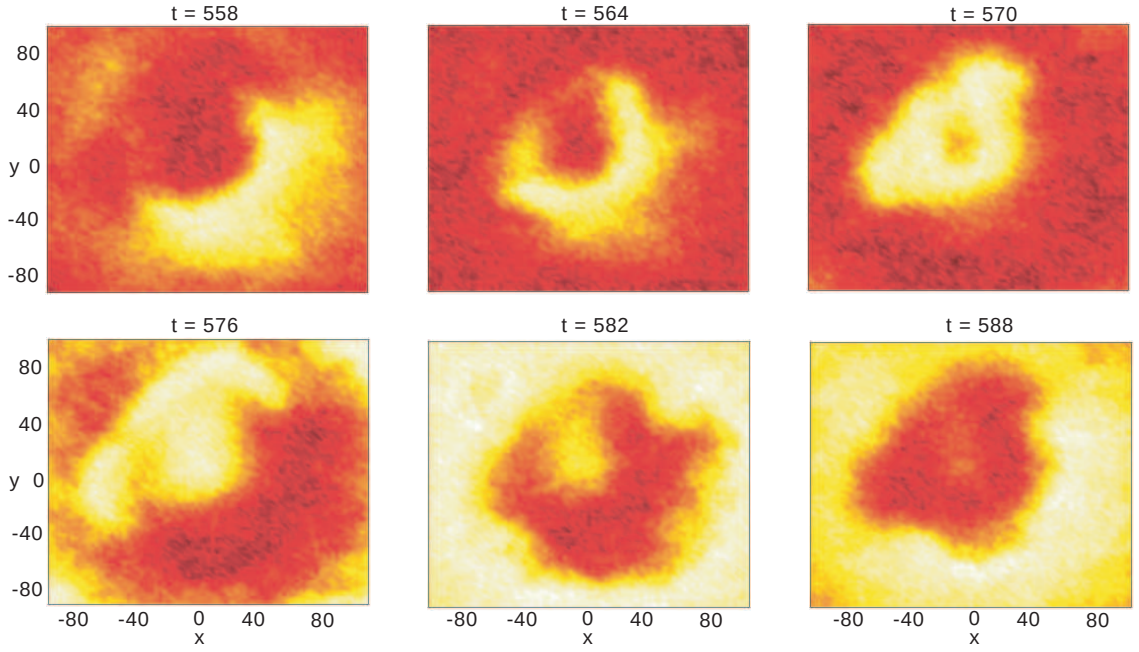

Fig. 11 Snapshots of a solution $u(x, y, t)$ to the noisy system (4.4), following a stimulus specified by equation (4.3) at $t = 90$, where $\chi = 1$ and $\zeta = 60$. As activity develops, the background noise starts to break the symmetry of an oscillating central core. Rather than a contiguous oscillation, two halves of the core oscillate antisynchronously. A semi-ring wave propagates from the bottom to the top of the medium, and breaks into two spiral waves as it collides with the boundary of the core. This exemplifies noise induced spiral waves, which are sustained for relatively long time intervals. Parameters are $\alpha = 80$, $\beta = 0.05$, $\eta = 0.01$, $\sigma = 4$, and $\theta = 0.01$.

tured activity in the network is disrupted and the entire network exhibits bulk oscillations. Indeed, it has previously been shown that there can be an optimal level of noise for the generation of spiral waves in excitable media [25]. Note that an alternative mechanism to noise for generating spiral waves is to introduce random network inhomogeneities (quenched disorder), as shown in the case of a two–dimensional integrate–and–fire network [39].

5 High-gain limit

In order to analyze the existence and stability of spatially structured solutions in neuronal networks, the high–gain limit of a sigmoid-like firing rate function is often considered, whereby f reduces to the Heaviside function (2.3) with a discontinuity at the threshold $u = \theta$ [2, 42]. Although an excitatory neuronal network with synaptic depression as given by equation (2.1) no longer supports oscillatory solutions in the high–gain limit, stationary pulses (bumps) and target wave solutions can be found. However, the presence of a Heaviside function in the dynamics of the synaptic depression variable means that the resulting dynamical system is piecewise smooth, which considerably complicates the analysis of the stability of waves and bumps. In this section, we carry out a phase–plane analysis of the space–clamped system, show that stable target wave solutions exist, and derive equations for the existence of stationary bumps. The issue of stability will be addressed elsewhere (see also [26]).

5.1 Phase-plane analysis

The space–clamped system with a Heaviside firing rate function takes the form

$$\begin{aligned} \dot{u}(t) &= -u(t) + q(t)H(u(t)-\theta), \\ \alpha\dot{q}(t) &= 1 - q(t) - \alpha\beta q(t)H(u(t)-\theta). \end{aligned} \tag{5.1}$$

In order to calculate equilibria of (5.1), we consider the possible solutions on the two domains of the step function $H(u-\theta)$. We find that there is always a low activity or Down state on the lower domain $(u < \theta)$ for $\theta > 0$ such that $(u, q) = (0, 1)$. The stability of this Down state is determined by the eigenvalues of the Jacobian

$$\mathcal{J}(0,1) = \begin{pmatrix} -1 & 0 \\ 0 & -1/\alpha \end{pmatrix} \tag{5.2}$$

and is therefore stable for all realistic parameters. As stated in our analysis of the system with the piecewise linear firing rate function, this stable Down state indeed should exist for all systems possessing an f with a hard threshold.

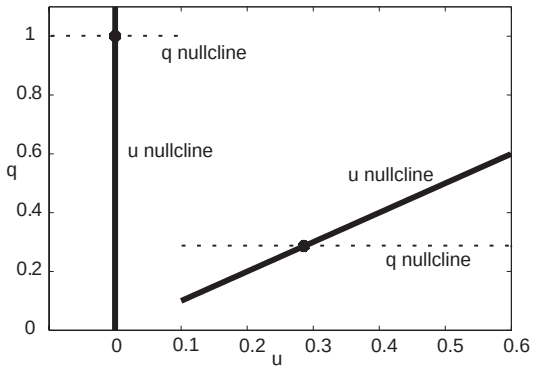

Fig. 12 Phase plane plot of the space-clamped system (5.1) fin the case $\theta < 1/(1+\alpha\beta)$ for which there exist two stable fixed points. Parameters are $\alpha = 50$, $\beta = 0.05$, and $\theta = 0.1$.

In the upper domain $(u > \theta)$, an equilibrium is given by the system

$$0 = -u + q, \tag{5.3}$$

$$0 = (1-q)/\alpha - \beta q, \tag{5.4}$$

implying a fixed point $(u,q) = (1/(1+\alpha\beta), 1/(1+\alpha\beta))$ will exist, provided $\theta < 1/(1+\alpha\beta)$. Its stability is determined by the eigenvalues of the Jacobian

$$\mathcal{J}(u,q,a) = \begin{pmatrix} -1 & 1 \\ 0 & -(1/\alpha+\beta) \end{pmatrix}, \tag{5.5}$$

which guarantees that such an Up state is always stable. Therefore, as stated, we have a bistable system as long as $\theta < 1/(1+\alpha\beta)$, as pictured in Fig. 12. Additive noise could then be a mechanism for switching the system between its Up and Down states. However, if $\theta > 1/(1+\alpha\beta)$, only the Down state exists, which physically means that in this case synaptic depression curtails recurrent excitation to the point that no sustained activity is possible. In the special case $\theta = 1/(1+\alpha\beta)$, an equilibrium exists at $u = q = \theta$, provided that we take $H(0) = 1$. However, the piecewise smooth nature of the dynamics needs to be taken into account in order to determine the stability of the fixed point. That is, the fixed point is stable with respect to perturbations $\delta u > 0$ but unstable with respect to perturbations $\delta u < 0$. Thus stability cannot be established simply by linearizing about the fixed point. While this special case is non-generic in the space–clamped system, it foreshadows potential problems in the study of the stability

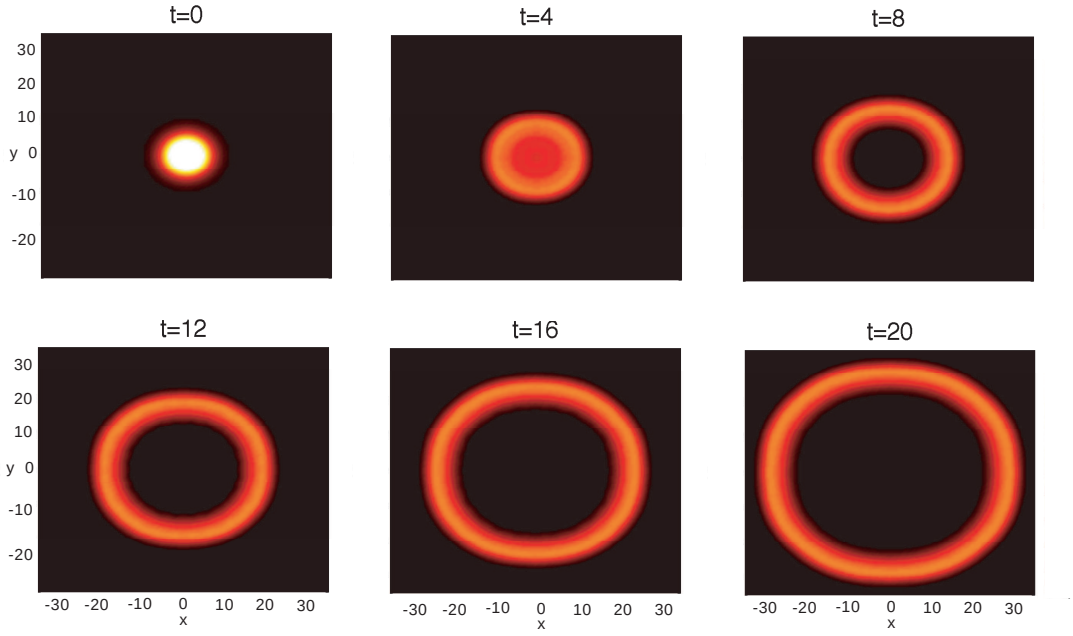

Fig. 13 Snapshots of a solution $u(x, y, t)$ to the fourth order PDE (4.1) showing a single outward propagating target wave, following a stimulus specified by equation (4.3) at $t = 0$, where $\chi = 1$ and $\zeta = 25$. The firing rate function is taken to be a Heaviside function, $f(u) = H(u - \theta)$. Parameters are $\alpha = 50$, $\beta = 0.4$, and $\theta = 0.1$.

of spatially structured solutions of the full system (2.1). This is due to the fact that one has to consider perturbations at threshold crossing points x where $u(x, t) = \theta$. We will discuss this issue further, following a study of spatially structured solutions.

5.2 Target waves

As shown by numerical simulations in the case of a piecewise linear firing rate, spatially structured oscillations can generate expanding target waves via propagating phase shifts in an oscillatory medium. Here, we show that in the high–gain limit, target waves arise in the context of an excitable medium. We studied the existence of traveling pulses in a one-dimensional excitatory network with synaptic depression in a previous study [26]. Traveling pulses of this type represent a homoclinic orbit in the projected space of the traveling wave coordinate, rather than phase shifts of an existing limit cycle, as in an oscillatory medium. Implications of these two different dynamical systems scenarios may be useful in determining the mechanism that generates traveling waves in experiment. For example, in studies of disinhibited cortical slice, localized stimuli may lead to either traveling plane waves, which are transient, or spiral waves, which are persistent [23].

We find that by simulating the two-dimensional spatially extended system with the Heaviside step firing rate function, a localized stimulus can lead to outwardly propagating target waves. In Fig. 13, we show snapshots of such a simulation where the initial condition is taken to be a Gaussian stimulus of the synaptic drive, as specified by equation (4.3). In the case of a piecewise linear firing rate function, radially symmetric stimuli lead to an oscillating core that recurrently generated target waves. Here, a single radially symmetric target wave is generated, after which, the system returns to a quiescent state. The structure of the solution reflects the underlying symmetries of the weight function (2.5) and the stimulus. Numerical simulations suggest that these target waves are stable.

5.3 Standing bumps

Finally, we extend our previous analysis of bumps in a one-dimensional network [26] in order to derive conditions for the existence of standing bumps in the two–dimensional network (2.1) with a Heaviside firing rate function. We can assume radially symmetric bumps since the corresponding weight distribution (2.5) is itself radially symmetric. Consider a radially symmetric stationary bump solution of equation (2.1) such that $u(\mathbf{r}, t) = U(r)$, $q(\mathbf{r}, t) = Q(r)$ and $U(r)$ crosses the threshold θ at

the unique radius $r = a$. The solution is taken to be superthreshold within the domain $r < a$ and subthreshold otherwise, and a is identified as the radial width of the bump. Given reasonable boundary conditions, we thus have

$$U(r) \gtrless \theta, \qquad \text{for } r \lessgtr a, \quad (5.6)$$

$$\{U(r), Q(r))\} \to \{0, 1\}, \qquad \text{as } r \to \infty. \quad (5.7)$$

Substituting such a solution into equation (2.1) gives

$$U(r) = \int_{\mathcal{U}} Q(r')w(|\mathbf{r} - \mathbf{r}'|)\mathrm{d}\mathbf{r}', \quad (5.8)$$

$$Q(r) = (1 + \alpha\beta\Theta(a - r))^{-1}, \quad (5.9)$$

where $\mathcal{U} = \{\mathbf{r} = (r, \theta) : r \leq a\}$ is the domain on which the bump is superthreshold and

$$\Theta(r) = \begin{cases} 1, & r \geq 0, \\ 0, & r < 0. \end{cases} \quad (5.10)$$

If we express (5.9) as

$$Q(r) = \begin{cases} \frac{1}{1+\alpha\beta}, & r \leq a, \\ 1, & r > a, \end{cases} \quad (5.11)$$

then we can substitute (5.11) back into (5.8) to yield

$$(1 + \alpha\beta)U(r) = \Pi(a, r), \quad (5.12)$$

where

$$\Pi(a, r) = \int_0^{2\pi} \int_0^a w(|\mathbf{r} - \mathbf{r}'|)r'\mathrm{d}r'\mathrm{d}\theta'. \quad (5.13)$$

We can calculate the double integral in (5.13) using Fourier transform and Bessel function identities, as in a previous study [14]. Thus, we find that

$$\Pi(a, r) = 2\pi a \int_0^\infty \hat{w}(\rho)J_0(r\rho)J_1(a\rho)\mathrm{d}\rho, \quad (5.14)$$

where $\hat{w}(\rho)$ is the two–dimensional Fourier transform of w, and $J_\nu(z)$ is a Bessel function of the first kind.

To illustrate the parameter dependence of stationary bumps, we consider the concrete example of a weight function w given by the difference of modified Bessel functions (2.5), which has the Fourier transform (4.2). The integral (5.14) can then be evaluated explicitly by substituting (4.2) into (5.14), setting $r = a$, and using the identity

$$a \int_0^\infty \frac{1}{\rho^2 + s^2} J_0(a\rho)J_1(a\rho)\mathrm{d}\rho = \frac{a}{s} I_1(sa)K_0(sa),$$

where I_ν is the modified Bessel function of the first kind. Thus, the condition for existence of a stationary bump of radius a is given by

$$(1 + \alpha\beta)\theta = \mathbf{\Pi}(a), \quad (5.15)$$

with

$$\mathbf{\Pi}(a) \equiv \Pi(a, a) = \frac{4}{3}\left(aI_1(a)K_0(a) - \frac{a}{2}I_1(2a)K_0(2a)\right). \quad (5.16)$$

Relations between bump radius a and depression strength β are shown in Fig. 14. Numerical simulations suggest all such bumps are unstable, so that some form of lateral inhibition is required in order to stabilize the bumps. Alternatively bumps could be stabilized by global divisive inhibition [61, 17]

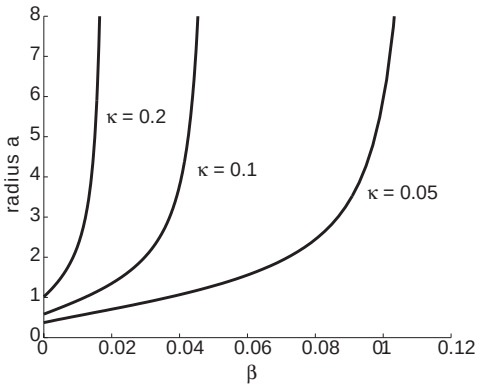

Fig. 14 Bump radius a as a function of depression strength β for different values of threshold θ, while $\alpha = 80$.

While bump existence calculations are straightforward in the case of a Heaviside firing rate function, bump stability calculations are not, due to the piecewise smooth nature of the depression dynamics. Following previous studies of bump stability [43, 14, 40], one could formally linearize the neural field equations. However, as we have recently shown in the case of one–dimensional bumps [26], considerable care has to be taken in evaluating terms arising from perturbations of the bump boundary. It turns out one needs to keep track of the *sign* of such perturbations, analogous to what happens when $\theta = 1/(1+\alpha\beta)$ in the space-clamped system. The details of this analysis will be presented elsewhere.

6 Discussion

In this paper, we analyzed the spatiotemporal dynamics of a two-dimensional excitatory neuronal network with synaptic depression. We showed that there is an extensive parameter range over which spatially structured oscillations are supported. With the inclusion of noise in the model this range is

widened even further. We found that application of a localized current input as an initial condition to the network leads to a localized region of synchronous activity repeatedly emitting target waves. This type of activity has been linked to epileptic seizures [8, 38], memory [27], and sensory input [31, 32, 45, 51]. Additionally, breaking the symmetry of target wave emitting solutions either using external stimulation or noise generated spiral waves. Disinhibited mammalian cortical slices also support spiral waves, and it has been postulated that such activity allows periodic activity to be organized in spatially extended populations of neurons [23, 48]. Finally, we showed that in the high–gain limit, the network acts like an excitable rather than oscillatory neural medium in which solitary target waves can propagate but stationary bumps are unstable.

Although the effects of short–term depression with and without noise have been studied in a variety of contexts [1, 57, 35, 53, 4, 22], its role in spatially structured networks has not previously been considered. Just as synaptic depression provides a negative feedback mechanism for generating moderately fast wave (1-10 Hz) oscillations, it is possible that synaptic facilitation of excitatory to inhibitory synapses plays a role in producing slow wave oscillations (0.1-1 Hz), as recently suggested by a modeling study of a space–clamped network [37]. We hope to pursue this in a future study.

Acknowledgements

This publication was based on work supported in part by the National Science Foundation (DMS-0813677) and by Award No KUK-C1-013-4 made by King Abdullah University of Science and Technology (KAUST). We would like to thank Carlo Laing for helpful conversations regarding numerical simulations. We also thank Bard Ermentrout for highlighting issues regarding bump stability calculations in the high–gain limit.

References

1. Abbott LF, Varela JA, Sen K, Nelson SB (1997) Synaptic depression and cortical gain control. Science 275: 220–224.
2. Amari S (1977) Dynamics of pattern formation in lateral-inhibition type neural fields. Biol. Cybern. 27: 77–87.
3. Bao S, Chang EF, Davis JD, Gobeske KT, Merzenich MM (2003) Progressive degradation and subsequent refinement of acoustic representations in the adult auditory cortex. J Neurosci. 23: 10765–10775.
4. Bart E, Bao S, Holcman D (2005) Modeling the spontaneous activity of the auditory cortex. J Comput. Neurosci. 19: 357–378.
5. Benda J, Herz AVM (2003). A universal model for spike-frequency adaptation, Neural Comput. 15: 2523–2564.
6. Benucci A, Frazor RA, Carandini M (2007) Standing waves and traveling waves distinguish two circuits in visual cortex. Neuron 55: 103-117.
7. Buszaki G, Draguhn A (2004) Neuronal oscillation in cortical networks. Science 304: 1926–1929.
8. Buszaki G (2006) Rhythms of the brain. Oxford University Press, Oxford.
9. Chervin RD, Pierce PA, Connors BW (1988) Periodicity and directionality in the propagation of epileptiform discharges across neocortex. J. Neurophysiol. 60: 1695–1713.
10. Delaney K, Gelperin A, Fee M, Flores J, Gervais R, Tank D (1994). Waves and stimulus-modulated dynamics in an oscillating olfactory network, Proc. Natl. Acad. Sci. USA 91: 669–73.
11. Dudek FE, Spitz M (1997) Hypothetical mechanisms for the cellular and neurophysiological basis of secondary epileptogenesis: Proposed role for synaptic reorganization. J. Clin. Neurophysiol. 14: 90–101.
12. Ermentrout GB (1998) Linearization of f-I curves by adaptation. Neural Comput. 10: 1721–1729.
13. Ermentrout GB, Kleinfeld D (2001) Traveling electrical waves in cortex: insights from phase dynamics and speculation on a computational role. Neuron 29: 33–44.
14. Folias SE, Bressloff PC (2004) Breathing pulses in an excitatory neural network. SIAM J. Appl. Dyn. Syst. 3: 378–407.
15. Folias SE, Bressloff PC (2005) Breathers in two-dimensional neural media. Phys. Rev. Lett. 95: 208107.
16. Folias SE, Bressloff PC (2005) Stimulus-locked traveling waves and breathers in an excitatory neural network. SIAM J. Appl. Math. 65: 2067–2092.
17. Fung CCA, Wong KYM, Wu S (2008) Dynamics of neural networks with continuous attractors. EPL 84: 18002
18. Guo Y, Chow CC (2005) Existence and stability of standing pulses in neural networks: I.

Existence. SIAM J. Appl. Dyn. Syst. 4: 217–248.
19. Guo Y, Chow CC (2005) Existence and stability of standing pulses in neural networks: II. Stability. SIAM J. Appl. Dyn. Syst. 4: 249–281.
20. Han F, Caporale N, Dan Y (2008). Reverberation of recent visual experience in spontaneous cortical waves, Neuron 60: 321–327.
21. Hansel D, Sompolinsky H (2001) Methods in Neuronal Modeling, The MIT Press, 2nd ed., ch. 13. Modeling feature selectivity in local cortical circuits: 499–568.
22. Holcman D, Tsodyks M (2006). The emergence of Up and Down states in cortical networks. PLoS Computational Biology. 2:174–181.
23. Huang X, Troy WC, Yang Q, Ma H, Laing CR, Schiff SJ, Wu JY (2004) Spiral waves in disinhibited mammalian neocortex. J. Neurosci. 24: 9897–9902.
24. Hutt A, Longtin A, Schimansky-Geier L (2008) Additive noise-induces Turing transitions in spatial systems with application to neural fields and the Swift-Hohenberg equation. Physica D 237: 755–773.
25. Jung P, Mayer-Kress G (1995). Spatiotemporal stochastic resonance in excitable media Phys. Rev. Let. 74: 2130 - 2133.
26. Kilpatrick ZP, Bressloff PC (2009) Effects of adaptation and synaptic depression on spatiotemporal dynamics of an excitatory neuronal network. Physica D (in press).
27. Klimesch W (1999) EEG alpha and theta oscillations reflect cognitive and memory performance: A review and analysis. Brain Res. Rev. 29: 169–195.
28. Laing CR, Troy WC (2003) PDE methods for nonlocal models. SIAM J. Appl. Dyn. Syst. 2: 487–516.
29. Laing CR (2005) Spiral waves in nonlocal equations. SIAM J Appl. Dyn. Syst. 4: 588–606.
30. Laing CR, Frewen TA, Kevrekidis IG (2007) Coarse-grained dynamics of an activity bump in a neural field model. Nonlinearity 20: 2127–2146.
31. Lakatos P, Chen CM, O'Connell MN, Mills A, Schroeder CE (2007) Neuronal oscillations and multisensory interaction in primary auditory cortex. Neuron 53: 279–292.
32. Lam YW, Cohen LB, Wachowiak M, Zochowski MR (2000) Odors elicit three different oscillations in the turtle olfactory bulb. J Neurosci. 20: 749–62.
33. Lee U, Kim S, Jung KY (2006) Classification of epilepsy types through global network analysis of scalp electroencephalograms. Phys. Rev. E 73: 041920.
34. Linder B, Garcia-Ojalvo, Neiman A, Schimansky-Geier L (2004) Effects of noise in excitable systems. Phys. Rep. 393: 321–424.
35. Matveev V, Wang XJ (2000) Implications of all-or-none synaptic transmission and short-term depression beyond vesicle depletion: a computational study. J Neurosci. 20: 1575–1588.
36. McNamara JO (1994) Cellular and molecular basis of epilepsy. J. Neurosci. 14: 3412–3425.
37. Melamed O, Barak O, Silberberg G, Markram H, Tsodyks M (2008) Slow oscillations in neural networks with facilitating synapses, J. Comput. Neurosci. 25:308-316.
38. Milton J, Jung P (2003) Epilepsy as a dynamic disease, Springer, Berlin.
39. Milton J G, Chu P H, Cowan J D (1993) Spiral waves in integrate-and-fire neural networks. In: Advances in neural information processing systems (Hanson SJ, Cowan JD, Giles CL, eds), pp 1001-1007. San Mateo: Morgan Kaufmann.
40. Owen MR, Laing CR, Coombes S (2007) Bumps and rings in a two-dimensional neural field: splitting and rotational instabilities. New Journal of Physics, 9: 378.
41. Petersen CCH, Grinvald A, Sakmann B (2003). Spatiotemporal dynamics of sensory responses in layer 2/3 of rat barrel cortex measured in vivo by voltage-sensitive dye imaging combined with whole-cell voltage recordings and neuron reconstructions, J Neurosci. 23 (4) 1298–1309.
42. Pinto DJ, Ermentrout GB (2001) Spatially structured activity in synaptically coupled neuronal networks: I. Traveling fronts and pulses. SIAM J. Appl. Math. 62: 206–225.
43. Pinto DJ, Ermentrout GB (2001) Spatially structured activity in synaptically coupled neuronal networks: II. Lateral inhibition and standing pulses. SIAM J. Appl. Math. 62: 226–243.
44. Prechtl JC, Cohen LB, Pesaran B, Mitra PP, Kleinfeld D (1997). Visual stimuli induce waves of electrical activity in turtle cortex, Proc. Natl. Acad. Sci. USA 94: 7621–7626.
45. Roelfsema PR, Engel AK, Konig P, Singer W (1997) Visuomotor integration is associated with zero time-lag synchronization among cortical areas. Nature 385: 1157–1161.
46. Rubin J, Bose A (2004) Localized activity patterns in excitatory neuronal networks. Network 15: 133–158.
47. Schiff SJ, Sauer T, Kumar R, Weinstein SL (2005) Neuronal spatiotemporal pattern discrim-

ination: The dynamical evolution of seizures Neuroimage 28: 1043-1055.
48. Schiff SJ, Huang X, Wu JY (2007) Dynamical evolution of spatiotemporal patterns in mammalian middle cortex. Phys. Rev. Lett. 98: 178102.
49. Sederberg PB, Kahana MJ, Howard MW, Donner EJ, Madsen JR (2003) Theta and gamma oscillations during encoding predict subsequent recall. J. Neurosci. 23: 10809-10814.
50. Shusterman V, Troy WC (2008) From baseline to epileptiform activity: a path to synchronized rhythmicity in large-scale neural networks. Phys. Rev. E 77: 061911.
51. Singer W, Gray CM (1995) Visual feature integration and the temporal correlation hypothesis. Ann. Rev. Neurosci. 18: 555-586.
52. Stevens C, Wesseling J (1998). Activity-dependent modulation of the rate at which synaptic vesicles become available to undergo exocytosis, Neuron 21 415–424.
53. Tabak J, Senn W, O'Donovan MJ, Rinzel J (2000) Modeling of spontaneous activity in developing spinal cord using activity-dependent depression in an excitatory network. J Neurosci. 20: 3041–3056.
54. Troy WC, Shusterman V (2007) Patterns and features of families of traveling waves in large-scale neuronal networks. SIAM J. Appl. Dyn. Syst., 6: 263–292.
55. Troy WC (2008) Traveling waves and synchrony in an excitable large-scale neuronal network with asymmetric connections. SIAM J. Appl. Dyn. Syst., 7: 1247–1282.
56. Tsodyks MS, Markram H (1997) The neural code between neocortical pyramidal neurons depends on neurotransmitter release probability. Proc. Natl. Acad. Sci. USA 94: 719–723.
57. Tsodyks MS, Pawelzik K, Markram H (1998) Neural networks with dynamic synapses. Neural Comput. 10: 821–835.
58. Wang XJ (1998) Calcium coding and adaptive temporal computation in cortical pyramidal neurons. J Neurophysiol. 79: 1549–1566.
59. Wang XJ (1999) Synaptic basis of cortical persistent activity: the importance of NMDA receptors to working memory. J. Neurosci. 19: 9587–9603.
60. Wu JY, Guan L, Tsau , Propagating activation during oscillations and evoked responses in neocortical slices. J Neurosci. 19: 5005–5015.
61. Wu S, Hamaguchi K, Amari S-I (2008) Dynamics and computation of continuous attractors. Neural Computation 20: 994–1025
62. Wu JY (2008) Propagating waves of activity in the neocortex: what they are, what they do. Neuroscientist 14: 487–502.
63. Xu W, Huang X, Takagaki K, Wu JY (2007) Compression and reflection of visually evoked cortical waves. Neuron 55: 119–129.
64. Zucker RS, Regehr WG (2002) Short–term synaptic plasticity. Ann. Rev. Physiol. 64: 355–405.